

Chapter 2

Overview of

Partition of Unity Methods

The work presented in this thesis can be characterized as the development of numerical methods for elliptic problems with local character. By ‘local character’ here, we allude to the solution in the vicinity of a local feature of interest, such as a line of discontinuity, a crack, or an interface. Regardless of the specific situation, the objective is to develop a method which captures the local character of the solution in a straightforward and efficient fashion.

In this chapter a few methods of constructing approximating spaces for the Galerkin method are presented, and the manner in which the basis functions form a partition of unity is reviewed. We also discuss the relative ease of constructing the shape functions and bilinear form. An approximate solution to a simple one-dimensional model problem is provided for each method to illustrate its key features. Emphasis is placed on the ability of the approximation to capture local features. The notations and conventions adopted throughout the remainder of the thesis are also introduced.

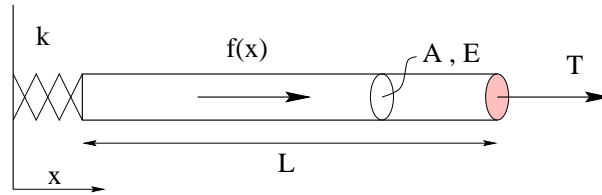


Figure 2.1: The one-dimensional model problem.

2.1 Model Problem

Consider the problem in one-dimensional linear elasticity of a bar of length L , subjected to a body force $f(x)$, and traction T at $x = L$ as shown in Fig. 2.1. The bar is constrained at the left end ($x = 0$) by a linear spring with constant k . For the sake of simplicity, we consider the case when the cross sectional area A and Young's modulus E are constant in the domain, and we take both values to be unity.

Having stated the assumptions, the boundary value problem (BVP) which describes the displacement $u(x)$ of the bar is given by

$$-u_{,xx} = f \quad \text{in } \Omega = (0, L) \quad (2.1a)$$

$$-ku(0) = -u_{,x}(0) \quad (2.1b)$$

$$u_{,x}(L) = T \quad (2.1c)$$

where a comma denotes a derivative with respect to the following subscript.

As stated previously, we are interested in problems with local character. We begin by considering the following choice for the body force $f \in L^2(\Omega)$:

$$f(x) = 6x + \left(\frac{2}{\alpha^2} - \left(\frac{L - 2x}{\alpha^2} \right)^2 \right) e^{-\left(\frac{x-L/2}{\alpha} \right)^2} \quad (2.2)$$

where the parameter α is chosen to be small in comparison to the length of the bar (i.e. $\alpha/L = 0.01$).

Neglecting the contributions from the exponential term on the boundary, the solution is given by

$$u(x) = (T + 3L^2)\left(\frac{1}{k} + x\right) - x^3 + e^{-\left(\frac{x-L/2}{\alpha}\right)^2} \quad (2.3)$$

Due to the exponential term in the body force, the solution has a local character about the center of the bar.

2.1.1 Variational Formulation

Let \mathcal{V} be a linear space. The variational boundary value problem (VBVP) which is equivalent to (2.1) is stated as follows: find the function $u \in \mathcal{V}$ that satisfies

$$a(u, v) = \langle l, v \rangle \quad \forall v \in \mathcal{V} \quad (2.4)$$

where $a : \mathcal{V} \times \mathcal{V} \rightarrow \mathcal{R}$ is the bilinear form

$$a(u, v) = \int_0^L u_{,x} v_{,x} dx + ku(0)v(0) \quad (2.5)$$

and $l : \mathcal{V} \rightarrow \mathcal{R}$ is the linear functional

$$\langle l, v \rangle = \int_0^L f v dx + Tv(L) \quad (2.6)$$

We note that since we have chosen a problem without essential boundary conditions, $\mathcal{V} = H^1(\Omega)$ is the space of admissible functions (as opposed to $H_0^1(\Omega)$). Here,

$H^m(\Omega)$ denotes the Sobolev space of order m , and $H_0^1(\Omega)$ denotes the same space of functions with vanishing values on the essential boundary. In the next section, we examine a few methods of constructing approximations to \mathcal{V} , and also comment on the construction of $a(u, v)$.

2.2 Galerkin methods

In this section, we briefly review the Galerkin method, and then present some specific approximations and their properties. The Galerkin method obtains approximate solutions to VBVPs by beginning with a finite dimensional subspace \mathcal{V}^h of \mathcal{V} spanned by N linear independent functions in \mathcal{V} . More precisely,

$$\mathcal{V}^h \subset \mathcal{V}, \quad \text{span}\{\varphi_i\}_{i=1}^N = \mathcal{V}^h \quad (2.7)$$

where φ_i are the basis functions. The parameter h is used to characterize the dimension of the subspace, and decreases as the number of basis functions N increases.

We now pose the VBVP (2.4) in \mathcal{V}^h as follows: find $u^h \in \mathcal{V}^h$ that satisfies

$$a(u^h, v^h) = \langle l, v^h \rangle \quad \forall v^h \in \mathcal{V}^h \quad (2.8)$$

In order to solve for the approximate solution u^h , we write

$$u^h(x) = \sum_{i=1}^N \varphi_i(x) u_i, \quad v^h(x) = \sum_{i=1}^N \varphi_i(x) v_i \quad (2.9)$$

and substitute these expressions into (2.8). Upon invoking the arbitrariness of the

values v_i , we obtain the system

$$\mathbf{K}\mathbf{u} = \mathbf{F} \quad (2.10)$$

where

$$K_{ij} = a(\varphi_i, \varphi_j) \quad (2.11a)$$

$$F_j = \langle l, \varphi_j \rangle \quad (2.11b)$$

In the following subsections, different methods of constructing the approximating space \mathcal{V}^h are presented. We also discuss the construction of the stiffness matrix \mathbf{K} . As a measure of the accuracy of the approximate solutions, we use the following L^2 and H^1 norms of the error

$$\|u - u^h\|_{L^2} = \left(\int_{\Omega} (u - u^h)^2 dx \right)^{1/2} \quad (2.12)$$

$$\|u - u^h\|_{H^1} = \left(\int_{\Omega} (u_{,x} - u_{,x}^h)^2 + (u - u^h)^2 dx \right)^{1/2} \quad (2.13)$$

and report normalized, or relative norms.

2.2.1 Finite element approximations

In this section, we review the construction of linear finite element approximations in one dimension. A few key properties are emphasized, such that comparisons can be made with the approximations presented in subsequent sections. For a more detailed

development, as well as the extension to higher dimensions, see Hughes (1987) or Szabo and Babuška (1991).

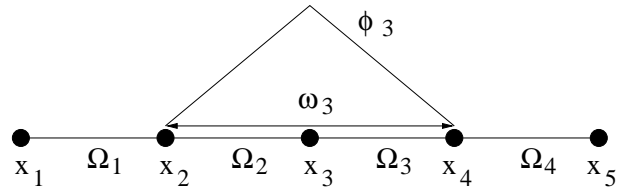


Figure 2.2: A typical one-dimensional mesh of 4 elements. A linear shape function ϕ for node 3 is shown, with support ω .

The construction of a finite element approximation begins by partitioning the domain Ω into a set of m subdomains, labeled elements. Nodes are then placed at the vertex of each element, for a total of n nodes in the domain. The coordinates of the nodes are denoted by x_1, x_2, \dots, x_n , and the element domains are denoted by $\Omega_1, \Omega_2, \dots, \Omega_m$. Associated with each node is a shape function ϕ_i , with compact support ω_i . The support of a nodal shape function is defined to be the union of the element subdomains connected to the node. Fig. 2.2 shows a nodal shape function and its support on a typical one-dimensional mesh.

The finite element basis functions are the nodal shape functions, which span a space of piecewise polynomials, of at least degree 1. A linear shape function is shown in Fig. 2.2. Higher order polynomial spaces can be constructed using internal degrees of freedom in conjunction with internal shape functions (Szabo and Babuška, 1991).

The finite element approximation reads

$$u^h(x) = \sum_{i=1}^n \phi_i(x) u_i \quad (2.14)$$

and we state the following properties, without proof:

- The approximation interpolates in the values u_i , ie $u^h(x_i) = u_i$.
- The approximation is continuous, $u^h \in C(\bar{\Omega})$.
- The approximation is linearly precise.

The interpolation property is attractive, as the nodal coefficients u_i take on a physical meaning; they are precisely the values of the displacement field at the nodes. The continuity of the approximation ensures that $\mathcal{V}^h \subset \mathcal{V}$, and is a direct result of the continuity of the shape functions. We note that constructing finite element shape functions with greater continuity is difficult in higher dimensions.

The linear precision of the approximation follows directly from the fact that the shape functions satisfy

$$\sum_i \phi_i(x) = 1, \quad \sum_i \phi_i(x)x_i = x \quad (2.15)$$

Hence, if the nodal values are prescribed according to an arbitrary linear field, the approximation (2.14) reproduces the field exactly. The above equations are often referred to as reproducing conditions, with the first implying that the shape functions form a *partition of unity* (Melenk and Babuška, 1996). This property corresponds to the ability of the approximation to represent rigid body modes, and is closely tied to the convergence of the method.

Concerning the construction of the stiffness matrix \mathbf{K} and force vector \mathbf{f} , the integrals over the domain Ω are replaced by a sum of integrals over each element subdomain Ω_i . An important feature of the finite element approximation is that the shape functions restricted to each element subdomain are polynomial functions. While these functions can be explicitly integrated, they are often integrated with

Gauss quadrature as the order can be selected to integrate the bilinear form (2.11a) exactly. In contrast, the exact evaluation of the force vector \mathbf{f} depends on the form of the body force. The usual convention is to replace the body force $f(x)$ by its projection on \mathcal{V}^h in (2.11b). We make a slight break in the following studies, and use high order Gauss quadrature in those element subdomains about the center of the bar to construct the force vector.

We now consider approximate finite element solutions to the model BVP (2.1). The data are taken to be $L = 1.0$, $T = -2$, and $k = 10$. The initial mesh consists of 19 elements and 20 nodes, evenly spaced on the domain $\Omega = (0, 1)$. The approximate solution is compared to the exact in Fig. 2.3. The finite element approximation clearly fails to capture the character of the solution about $x = 0.5$, which is not surprising as the local feature is contained within a single element. The approximate solution can be improved by refining the discretization, but we must add new elements and new nodes. While remeshing is trivial in one dimension, the process is expensive for two and three-dimensional analyses.

Table 2.1 summarizes the results for three finite element discretizations. The error does not always decrease with increased discretization, as a certain amount of *mesh-dependency* is observable. There is a marked decrease in accuracy associated with the mesh of 39 elements in comparison to that with 38 elements. In the former case, a node is located at the center of the bar, while in the latter case the point $x = 0.5$ is located in an element center. To a certain extent, the difficulties associated with remeshing and the problems of mesh-dependency provided motivation for the development of meshless methods.

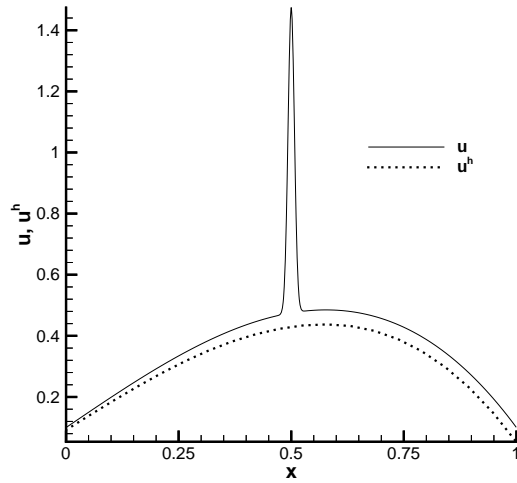


Figure 2.3: The finite element and exact solution for the model problem.

Table 2.1: Finite element results for model problem.

elements	$h = \Delta x$	L^2 error norm	H^1 error norm
19	0.0526	0.31	0.99
38	0.0263	0.12	0.63
39	0.0256	0.21	0.98

2.2.2 Meshless approximations

Meshless methods seek to circumvent the difficulties associated with mesh topology by constructing an approximation entirely from nodal data. Consider the domain $\Omega \subset \mathcal{R}$ and a set of n scattered nodes with coordinates $\{x_1, x_2, \dots, x_n\} \in \bar{\Omega}$. The construction of the meshless approximation begins with a set of weight functions $w_i(x)$ associated with the nodes. The nodal weight functions have compact support $\omega_i \subset \Omega$, and are constructed from a positive scalar valued function. For example, consider the following quartic function

$$w(r) = \begin{cases} 1 - 6r^2 + 8r^3 - 3r^4 & \text{for } 0 \leq r \leq 1 \\ 0 & \text{for } r > 1 \end{cases} \quad (2.16)$$

Defining the distance $d_i = |x - x_i|$, the nodal weight functions are given by

$$w_i(x) = w\left(\frac{d_i}{d_{mi}}\right) \quad (2.17)$$

where d_{mi} is computed using a global support multiplier s_m ;

$$d_{mi} = s_m c_i \quad (2.18)$$

The distance c_i is characteristic of the nodal spacing about node i . The support of the weight functions, ω_i is therefore

$$\omega_i = (x_i - s_m c_i, x_i + s_m c_i) \quad (2.19)$$

This subset of the domain is often referred to as a node's domain of influence.

The use of the nodal weight functions as a basis for \mathcal{V}^h does not generally lead to convergence for second order problems when the resulting approximation is not linearly precise. Meshless methods therefore construct shape functions $\{\phi_i\}$ from the nodal weight functions such that the reproducing conditions (2.15) are satisfied. This construction takes various forms; the following development is consistent with both the EFG (Belytschko et al., 1994) and RKPM (Liu et al., 1995) formulations.

Consider the meshless shape functions ϕ_i to be the nodal weight functions multiplied by a correction function:

$$\phi_i(x) = (C_1(x) + C_2(x)x_I)w(x - x_i) = \mathbf{C}(x)^T \mathbf{p}(x_i)w(x - x_i) \quad (2.20)$$

where $\mathbf{C}(x)^T = [C_1 \quad C_2]$ and $\mathbf{p}(x)^T = [1 \quad x]$ is a linear basis. By substituting the above form into the reproducing conditions (2.15), the following system of equations results for the coefficients $\mathbf{C}(x)$:

$$\mathbf{C}(x) = \mathbf{A}(x)^{-1} \mathbf{p}(x) \quad (2.21)$$

where

$$\mathbf{A}(x) = \left[\sum_{i \in N} w(x - x_i) \begin{bmatrix} 1 & x_i \\ x_i & x_i^2 \end{bmatrix} \right] \quad (2.22)$$

The shape functions then satisfy (2.15) by construction, provided that \mathbf{A} is invertible. This is guaranteed by setting the distances c_i appropriately. A typical one-dimensional meshless shape function is shown in Fig. 2.4. We note that the support of the shape function is equal to that of the nodal weight function.

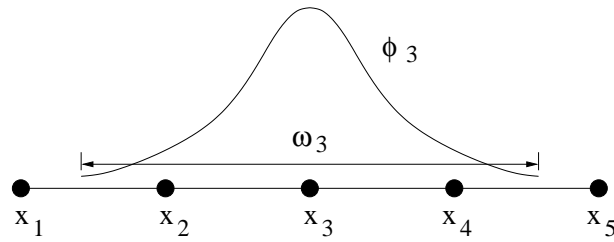


Figure 2.4: A typical meshless shape function ϕ , with support ω .

The meshless approximation reads

$$u^h(x) = \sum_i \phi_i(x)u_i \quad (2.23)$$

and we state the following properties, without proof

- The approximation is $C^k(\Omega)$ continuous, where $k = \min\{C^w(\Omega), C^p(\Omega)\}$.
- The approximation is linearly precise.
- The approximation does not interpolate in the values u_i , ie $u^h(x_i) \neq u_i$.

where C^w is the continuity of the nodal weight functions and C^p is the continuity of the basis (Lancaster and Salkauskas, 1981). The ease of constructing approximations with a high degree of continuity is quite useful when the admissible space is $H^2(\Omega)$ (see Chu and Moran (1995), for example). The precision of the approximation follows directly from the conditions (2.15). The lack of interpolation is often cited as a factor contributing to the difficulties associated with meshless approximations and the satisfaction of essential boundary conditions.

The accurate integration of the basis functions for the construction of the stiffness matrix is not as trivial as for finite element approximations. Firstly, the shape functions ϕ_i are not generally polynomial functions due to the correction (2.20). Secondly,

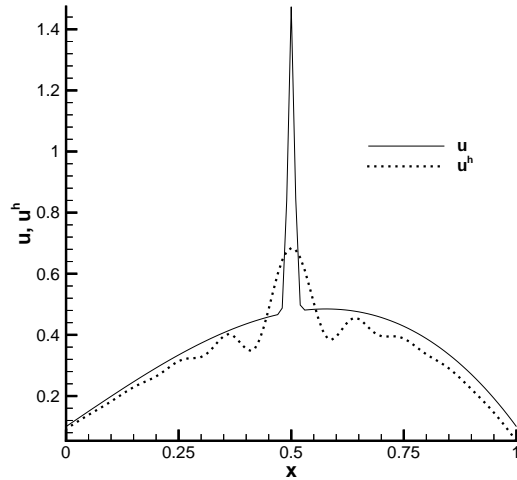


Figure 2.5: The meshless and exact solution for the model problem.

the support of the shape functions are not associated with any element subdomains. The standard approach is to partition the domain into a set of background cells, and to then use Gauss quadrature in each cell. For low-order quadrature, this approach can lead to significant errors in the construction of the bilinear form (Dolbow and Belytschko, 1999). In the following studies, we use high-order Gauss quadrature (10 pt) in the background cells to construct both the stiffness matrix and force vector.

Fig. 2.5 shows the meshless and exact solutions using the same data as in the previous section. The meshless approximation is constructed using 20 evenly spaced nodes in Ω , with the support multiplier $s_m = 2.2$. For each node, the distance c_i is set to be the distance to the second nearest neighbor node. For a uniform nodal arrangement, this is sufficient to ensure that \mathbf{A} is invertible in Ω . The bilinear form is constructed with background quadrature, where the integration cells are set from the nodal spacing. The meshless solution clearly captures more of the local solution about

Table 2.2: Meshless results for model problem.

nodes	h	L^2 error norm	H^1 error norm
20	0.0526	0.24	0.98
39	0.0263	0.11	0.76
40	0.0256	0.15	0.89

$x = 0.5$ than the finite element solution. In comparing Table 2.2 with Table 2.1, a slight increase in accuracy and a slight decrease in mesh dependency is also observable.

The construction of a meshless approximation is more expensive than a finite element approximation, due to the need to solve a system of equations at every point in the domain. An additional expense is associated with the high-order quadrature required to construct the stiffness matrix accurately. For the additional computational cost, a marginal amount of improvement is observable in the approximate solution. The development of finite element approximations with local enrichment improves the accuracy of the standard formulation, without the additional computational cost associated with meshless approximations.

2.2.3 Finite element approximations with local enrichment

The concept of incorporating local enrichment in an approximation through the finite element partition of unity was introduced in Melenk and Babuška (1996). The essential feature is the multiplication of the enrichment functions by nodal shape functions. The enrichment is able to take on a local form by only enriching those nodes whose support intersect a region of interest.

We denote by I the set of all n nodes in the domain, and by J the subset of I corresponding to the n^E enriched nodes. The finite element approximation with

enrichment reads

$$u^h(x) = \sum_{i \in I} \phi_i(x) u_i + \sum_{i \in J} \phi_i(x) \sum_{j=1}^{n^{Ei}} g_j(x) a_{ji} \quad (2.24)$$

where u_i and a_{ji} are nodal degrees of freedom, and n^{Ei} denotes the number of enrichment functions for node i . We state the following properties

- The approximation is $C^k(\Omega)$ continuous, where $k = \min\{C^s(\Omega), C^e(\Omega)\}$.
- The approximation is linearly precise.
- The approximation does not interpolate in the coefficients u_i on Ω .

In the above, the continuity of the shape functions and enrichment functions are denoted by $C^s(\Omega)$ and $C^e(\Omega)$, respectively. The form of the approximation as a sum of the standard plus enrichment terms ensures that linear precision is retained in the coefficients u_i . By the same token, if $i \in J$ then $u^h(x_i) = u_i + \sum_j g_j(x_i) a_{ji}$ and interpolation in the nodal values u_i is lost in enriched regions.

The enriched approximating space is formed from the union of the set of nodal shape functions with the set of products of shape functions and enrichment functions. In other words,

$$\mathcal{V}^h \equiv \text{span}\{\varphi_i\}_{i=1}^N \quad (2.25)$$

where the enriched basis is given by

$$\{\varphi_i\}_{i=1}^N = \{\phi_i\}_{i=1}^n \cup \{\phi_j g_1, \phi_j g_2 \dots \phi_j g_{n^{Ej}}\}_{j=1}^{n^E} \quad (2.26)$$

To see how the enriched basis functions are realized locally, consider the case when all nodes whose support intersect a region $D \subset \Omega$ are enriched with the function $g_1(x)$. If the only non-zero nodal coefficients are a_{1i} , we can write

$$u^h(x) = \sum \phi_i(x) g_1(x) = g_1(x) \quad \text{if} \quad a_{1i} = 1 \quad \forall i \quad (2.27a)$$

$$u^h(x) = \sum \phi_i(x) x_i g_1(x) = x g_1(x) \quad \text{if} \quad a_{1i} = x_i \quad \forall i \quad (2.27b)$$

as the finite element shape functions satisfy the reproducing conditions (2.15). By selecting the region D and the function $g_1(x)$ appropriately, the approximation is able to capture local features in the solution in a straightforward and efficient fashion.

From the preceding development it can be seen that the enrichment functions g_j cannot be selected arbitrarily, especially if the approximation is to be substituted into the bilinear form (2.11a). For the shape functions and enrichment functions to form a basis for \mathcal{V}^h , they must be linearly independent. This precludes enrichment with constant or linear functions, for example, as well as pairs of functions g_j which are linearly dependent. The substitution of approximations with linear dependencies into the bilinear form results in a stiffness matrix \mathbf{K} which is not invertible.

The construction of the bilinear form (2.11a) proceeds much in the same way as for the standard finite element approximation. The support of both the standard and enriched basis functions are unions of element subdomains, and so the integral over the domain can be replaced with a sum of integrals over the element subdomains. Some care must be taken to integrate the contribution from the enriched functions $g_j(x)$, especially when they are not polynomials. In comparison to meshless approximations, the process is aided considerably as the form of the basis functions are known explicitly, and their supports are defined by a union of element subdomains.

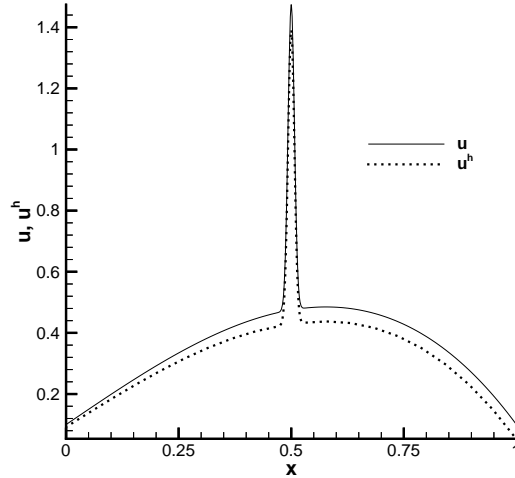


Figure 2.6: The generalized finite element and exact solution for the model problem.

We now discuss the construction of an enriched approximation appropriate for the model BVP. By examining the form of the body force, we enrich only those nodes about the center of the bar with the function

$$g_1(x) = e^{-\left(\frac{x-L/2}{\alpha}\right)^2} \quad (2.28)$$

We note that this is a local function in the sense that $g(x)$ and its derivative approach zero very quickly away from the center of the bar. The set of nodes J enriched with this function is taken to be

$$J = \{j \in I : \omega_j \cap D \neq \emptyset\} \quad (2.29)$$

where D is the interval $(9/19, 10/19)$ on the real line. This interval is chosen such that for the initial partition of the domain with 19 elements, a node on each side of

Table 2.3: Enriched finite element results for model problem.

nodes	#dof	L^2 error norm	H^1 error norm
20	22	0.10	0.037
39	42	0.00053	0.0023
40	44	0.00051	0.0022

$x = L/2$ is enriched with $g_1(x)$.

Fig. 2.6 shows the solution using the enriched approximation, which clearly captures the local character about $x = 0.5$. The results are not surprising, as information about the solution has been incorporated into the approximation. Table 2.3 summarizes the results for three different discretizations, where the number of degrees of freedom (#dof) is also provided. As the approximation is refined, we do not see the mesh dependency observed for the standard method.

Convergence results for the three methods presented in this section are shown in Fig. 2.7. For each discretization, the value of h is set to be $1/N$ where N is the dimension of \mathcal{V}^h . The enriched finite element approximation is clearly the most accurate, exhibiting a high initial rate of convergence. We note that the convergence of the enriched approximation behaves very similarly to that of higher order p -element approximations to singular problems (Szabo and Babuška, 1991). However, the leveling-off in convergence rate may be attributed to the fact that the accuracy of the enriched solution is very close to machine precision for small h .

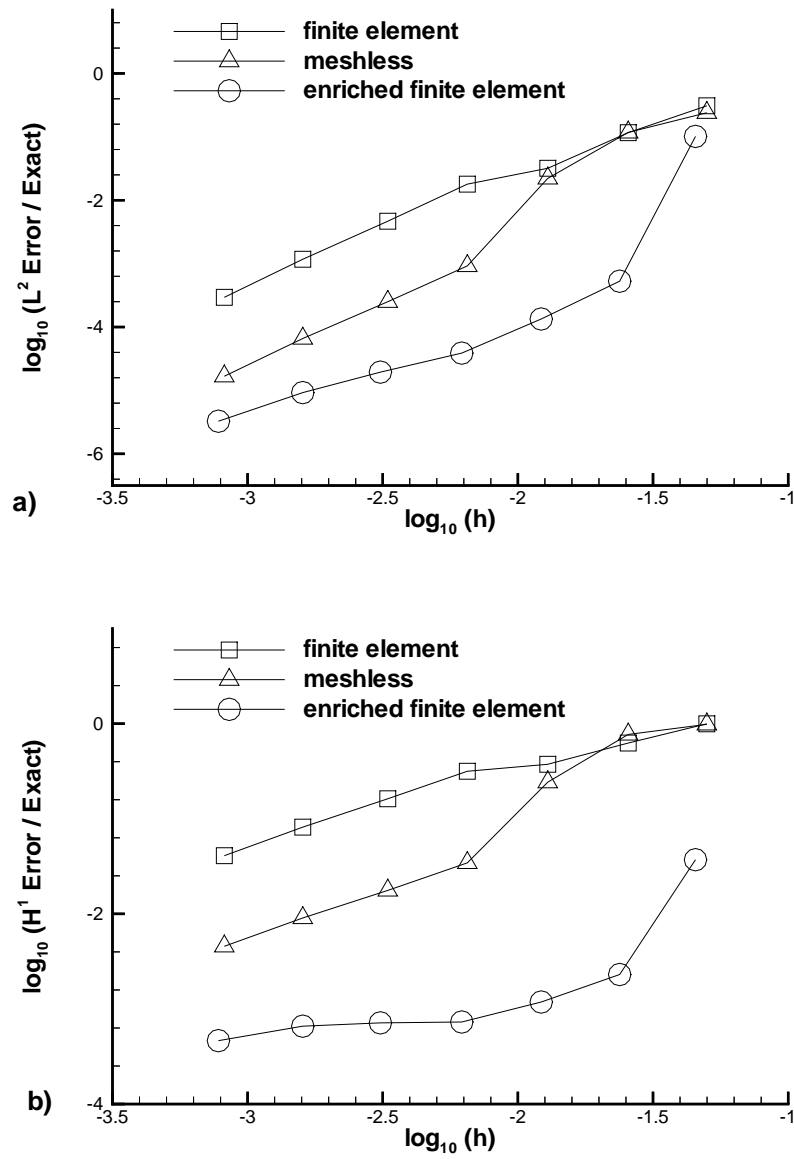


Figure 2.7: Convergence results in the a) L^2 norm and b) H^1 norm.

2.3 Closing Remarks

This chapter examined the ability of finite element and meshless approximations to capture a solution with local character. While approximate solutions for a specific boundary value problem were considered, the observed difficulties are characteristic of the methods on the whole. Finite element approximations often exhibit mesh-dependencies and poor accuracy for these classes of problems, while meshless methods incur a significantly greater computational expense. In this context, the advantages of a finite element formulation with local enrichment are obvious. By incorporating local enrichment functions, the enriched approximation is capable of accurately capturing local features of the solution in a straightforward and robust fashion. As the approximation is only modified locally, the overall computational expense is much less than that of a meshless method.

A legitimate criticism of the enriched formulation concerns the assumption of some knowledge about the solution. In this chapter, for example, a specific exponential term was included in the basis because the exact form of the solution was known *a priori*. In general this amount of insight into the solution may not be available. The next chapter presents the incorporation of discontinuous enrichment in the finite element framework, with applications to modeling cracks and crack growth. For these problems the only knowledge required about the solution is that it is discontinuous across a given line or surface. Emphasis is placed on the ease of representing the crack geometry independently of the finite element mesh. It will be shown in the chapters which follow that a finite element approximation with local enrichment is capable of capturing the discontinuity in a very robust and consistent fashion.